

Strong orbital correlations in a Fe-substituted spin-glass-manganite

E. Granado,^{1,2,*} R. R. Urbano,¹ C. A. Pérez,² C. Azimonte,^{1,2} J. W. Lynn,^{3,4} R. A. Souza,^{1,2} N. M. Souza-Neto,^{1,2} A. Y. Ramos,² G. L. Bychkov,⁵ S. V. Shiryayev,⁵ and S. N. Barilo⁵¹Instituto de Física “Gleb Wataghin,” UNICAMP, C.P. 6165, 13083-970, Campinas, SP, Brazil²Laboratório Nacional de Luz Síncrotron, C.P. 6192, 13084-971, Campinas, SP, Brazil³NIST Center for Neutron Research, National Institute of Standards and Technology, Gaithersburg, Maryland 20899, USA⁴Center for Superconductivity Research, University of Maryland, College Park, Maryland 20742, USA⁵Institute of Solid State and Semiconductor Physics, Academy of Sciences, 220072 Minsk, Belarus

(Received 2 May 2005; published 22 August 2005)

The compound $\text{La}_{0.66}\text{Ba}_{0.40}\text{Mn}_{0.61}\text{Fe}_{0.33}\text{O}_3$ shows anisotropic magnetic correlations with no long-range order. Specific heat measurements suggest these correlations represent the bulk. Orbital correlations of $\text{Mn}^{3+}e_g$ electrons, surviving in an environment of largely disordered exchange interactions, are invoked to account for this magnetic state. These results argue in favor of a strain-field mechanism for orbital ordering in manganites.

DOI: 10.1103/PhysRevB.72.052406

PACS number(s): 75.50.Lk, 61.10.-i, 61.12.-q, 78.70.Dm

The so-called orbital degree of freedom is an essential ingredient to the physics of transition-metal compounds.¹ There is consensus that orbital order (OO) strongly influences the exchange interactions and by extension the magnetic order in manganites (a prototype system) and other transition-metal oxides.² However, the converse, i.e., the role of electronic exchange as a possible driving mechanism of OO,³ is still under debate. The alternative mechanism arises from the anisotropic elastic field⁴ due to the Jahn-Teller effect in Mn^{3+} ions that may couple the underlying lattice distortions and lead to OO. In this work, the nature of OO in manganites is investigated in a three-dimensional manganite in the relatively dilute orbital regime, by means of a dense high-spin Fe^{3+} -substitution that affects differently the electronic exchange and the elastic field interactions. An interesting frustrated magnetic state with anisotropic magnetic correlations is observed. Such correlations are argued to be bulk-representative by the analysis of low T specific-heat data. Orbital physics is invoked to understand such correlations in a quasi-cubic system. Also, conspicuous thermal behaviors of the lattice parameters and bond distances seem to insinuate a long-range OO component. These results taken together, in a system with a large degree of chemical/exchange disorder, argue in favor of a strain-field mechanism for OO in manganites.

A crystal of $\text{La}_{0.66(4)}\text{Ba}_{0.40(2)}\text{Mn}_{0.61(3)}\text{Fe}_{0.33(2)}\text{O}_3$ (LBMF) weighing ~ 0.5 g was grown from a high-temperature flux.⁵ The cationic concentrations were determined from synchrotron x-ray fluorescence spectroscopy measurements using a monochromatic beam of 8 keV and employing the fundamental parameter method.⁶ A characterization of the bulk properties of LBMF was performed, aimed to guide our microscopic neutron and synchrotron x-ray investigation. Figure 1(a) shows the resistivity of LBMF between 100 K and 300 K, obtained with a four-contact configuration. Below 100 K down to 2 K, the resistivity values remain too high to be measured in our apparatus. A simple semiconducting-like behavior was found in the studied T interval. Figure 1(b) shows specific heat data below 180 K (symbols), taken using a standard thermal relaxation technique. No sharp peaks in-

dicative of a transition to long-range order were observed. The low T limit of C/T is given in Fig. 1(c) (symbols), with a dominant linear contribution. The dc-magnetic susceptibility was measured with a Superconducting Quantum Interference Device magnetometer [see Fig. 1(b)], showing a broad peak at $T_f \sim 53$ K. The nature of the feature at T_f was further investigated by ac-susceptibility measurements taken with a

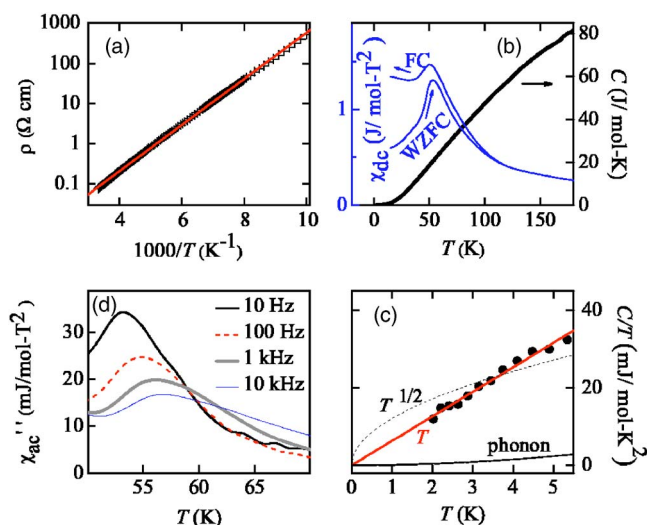


FIG. 1. (Color online) (a) Resistivity of $\text{La}_{0.66}\text{Ba}_{0.40}\text{Mn}_{0.61}\text{Fe}_{0.33}\text{O}_3$ as a function of the inverse T (symbols), and a fit to a semiconducting behavior with activation energy $\epsilon=0.11$ eV (solid line). (b) T dependence of the specific heat $C(H=0)$ (thick solid line) and dc-magnetic susceptibility $\chi_{dc}(H=0.01$ T) taken on field cooling (FC) and warming after zero field cooling (WZFC) (thin solid lines). (c) C/T vs. T in the low T limit (symbols), highlighting the dominant contribution due to the lowest power term in T , and tentative fits to square-root and linear behaviors due to gapless spin excitations in a ferromagnet (dashed curve) and a layered A-type antiferromagnet (solid line) (Ref. 9), respectively. The estimated phonon contribution, using $\theta_{Debye} \sim 275$ K (Ref. 9), is also given. (d) Out-of-phase ac-magnetic susceptibility for several frequencies in a selected T interval, taken with a field amplitude of 1 mT.

commercial platform. Figure 1(d) shows the out-of-phase signal χ'' for several frequencies. A maximum in χ'' is observed, providing evidence for a magnetic transition at T_f not revealed by the specific heat. As the frequency increases, the maximum in χ'' becomes less prominent and shifts to higher temperatures, indicating a transition to a glassy state without long-range magnetic order, such as a spin-glass⁷ or a cluster-glass state. The in-phase signal χ' (not shown) is similar in shape to the WZFC dc curve given in Fig. 1(b), with a decrease of $\sim 10\%$ in the peak height as the frequency increases from 10 Hz to 10 kHz.

Further details of the magnetic state of LBMF are provided by neutron-scattering experiments (see Ref. 8 for a description of the experimental setup). Reciprocal-space scans along the $(h00)$, $(hh0)$, and (hhh) directions were taken at 10 K and 300 K (not shown). The (hkl) indexing is defined here with respect to the pseudo-cubic unit cell ($a \sim 3.9$ Å). Neither magnetic intensities on existing Bragg peaks nor sharp superstructure peaks, which might be associated with long-range magnetic or charge ordering of any kind, were observed down to 10 K, within our experimental sensitivity. Energy scans for a typical wavevector $Q=(0.9,0,0)$ capturing diffusive scattering are given in Fig. 2(a) at 10 K and 200 K. At 200 K, a quasi-elastic paramagnetic scattering is observed, which disappears at low T , converting into an elastic diffusive signal. This is consistent with the development of a magnetically frustrated phase on cooling. Q -scans at 10 K and 300 K, both elastic and inelastic with neutron energy loss of 1.5 meV (not shown), confirmed that the scattering nearby $Q=(0.9,0,0)$ is not part of any peak or broad feature, being mostly due to uncorrelated spins. Figure 2(b) shows the T dependence of the quasi-elastic scattering at $Q=(0.9,0,0)$ and $\delta E=1.5$ meV, revealing that the spin-freezing occurs below T_f , consistent with magnetic susceptibility measurements [see Figs. 1(b) and 1(d)]. Additionally, relatively broad features centered at $(h+1/2,k,l)$ (h, k, l integers) were observed at low T . The intensities of these peaks decrease for increasing scattering vectors, consistent with their magnetic nature. Energy scans at $(1/2,0,0)$ (not shown) indicate that this scattering is elastic at 10 K, within our experimental resolution. This result reveals static layered (A-type) AFM correlations in LBMF. Transverse elastic scans in reciprocal space crossing the $(1/2,0,0)$ point are shown in Fig. 2(c) at selected T . Figure 2(d) shows the T dependence of the integrated intensity of the A-AFM $(1/2,0,0)$ peak. The correlation length ξ , obtained from the width of this reflection, is also given in Fig. 2(d). The A-AFM static correlations were not observed above ~ 160 K, while ξ decreases linearly with T , from 33(2) Å at 10 K to 10(5) Å at 150 K. These correlations are possibly the cause of the linear behavior of C/T at low T [see Fig. 1(c)], consistent with gapless spin excitations of an A-type AFM spin structure such as in LaMnO_3 .⁹

A powdered sample was obtained from crystallites grown in the same batch as the ~ 0.5 g crystal. High-resolution neutron and synchrotron x-ray powder diffraction data confirmed the absence of long-range charge or magnetic order. For experimental details, see Ref. 10. The T dependencies of the lattice parameters of LBMF between 10 K and 650 K are

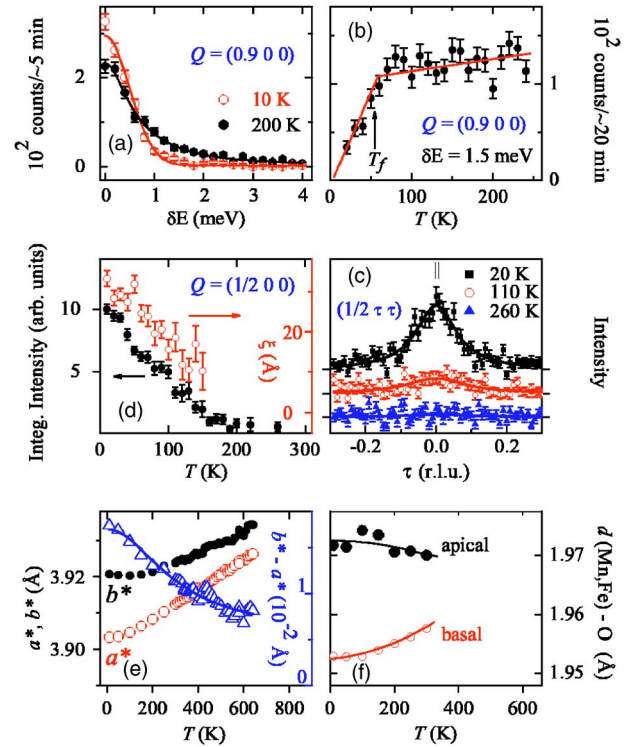


FIG. 2. (Color online) (a) Inelastic neutron scattering of $\text{La}_{0.66}\text{Ba}_{0.40}\text{Mn}_{0.61}\text{Fe}_{0.33}\text{O}_3$ at fixed $Q=(0.9,0,0)$ (cubic notation), taken at 10 K (open symbols) and 200 K (filled symbols), as a function of neutron energy loss. (b) T dependence of the scattering at $Q=(0.9,0,0)$ and $\delta E=1.5$ meV. (c) Elastic transverse scans across the reciprocal lattice point $(1/2,0,0)$ at selected T . The instrumental+mosaic width is indicated by short vertical bars. Data at different T were vertically translated for clarity. (d) T dependence of the integrated intensity of the A-AFM $(1/2,0,0)$ peak. The correlation length ξ , obtained from the width of this reflection, is also given in Fig. 2(d). The A-AFM static correlations were not observed above ~ 160 K, while ξ decreases linearly with T , from 33(2) Å at 10 K to 10(5) Å at 150 K. These correlations are possibly the cause of the linear behavior of C/T at low T [see Fig. 1(c)], consistent with gapless spin excitations of an A-type AFM spin structure such as in LaMnO_3 .⁹

given in Fig. 2(e). The data are presented in terms of the “pseudo-cubic” perovskite unit cell, $a^* \equiv a/\sqrt{2} \equiv c/\sqrt{2}$ and $b^* \equiv b/2$. Figure 2(e) also shows the thermal evolution of $b^* - a^*$. A clear separation of b^* and a^* as T decreases can be noticed. In principle, this behavior might originate from either crystallographic or electronic effects. Below we argue against the first possibility. In fact, the high resolution of our synchrotron x-ray diffraction data allows us to ascertain that no symmetry-driven transition occurred in the studied T interval. Instead, the separation of b^* and a^* changes more rapidly between ~ 100 K and ~ 400 K and does not appear to collapse at higher T as would be expected for a symmetry-driven crystallographic phase transition. The thermal behavior of $b^* - a^*$ is more suggestive of an OO state below ~ 300 – 500 K, possibly convoluted with smooth rotations of

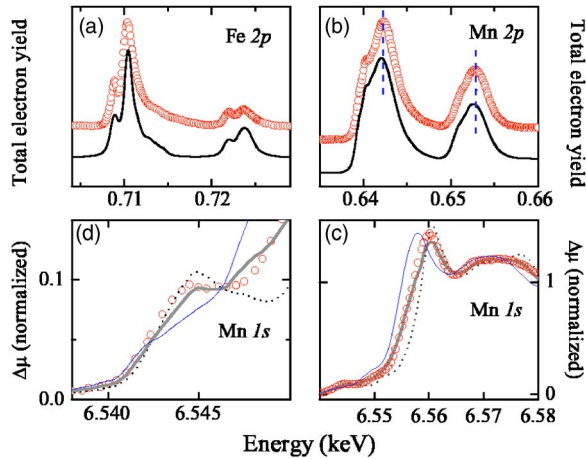


FIG. 3. (Color online) (a) Fe $2p$, (b) Mn $2p$, and (c,d) Mn $1s$ x-ray absorption near-edge structure (XANES) spectra of $\text{La}_{0.66}\text{Ba}_{0.40}\text{Mn}_{0.61}\text{Fe}_{0.33}\text{O}_3$ (symbols). The solid line in (a) displays a crystal-field multiplet simulation (Ref. 12), assuming a high-spin $\text{Fe}^{3+}:t_{2g}^3e_g^2$ ground state. The solid line in (b) is the Mn $2p$ XANES spectrum of $\text{La}_{0.7}\text{Sr}_{0.3}\text{MnO}_3$. The Mn $1s$ XANES spectra of LaMnO_3 and CaMnO_3 reference samples are given in (c,d) as thin solid and dashed lines, respectively, while the combination $0.55 \times \mu(\text{CaMn}^{4+}\text{O}_3) + 0.45 \times \mu(\text{LaMn}^{3+}\text{O}_3)$ is given as thick solid lines.

the oxygen octahedra. This perception seems to be further reinforced by the (Mn,Fe)—O bond distances [see Fig. 2(f)], with the (Mn,Fe)— O_{apical} distance (along b direction) being larger than the (Mn,Fe)— O_{basal} distance (in the ac plane) below room temperature. However, the distortion is relatively small, thus long-range OO cannot be unequivocally established on the basis of the diffraction data presently at hand.

Before proceeding with a discussion of the above results, an unambiguous identification of the electronic states of the Mn and Fe ions is required. The $2p$ soft x-ray absorption spectrum of Fe in LBMF is given in Fig. 3(a), which is very similar to that reported for LaFeO_3 ,¹¹ and in line with a crystal-field multiplet calculation¹² for high-spin Fe^{3+} [solid line in Fig. 3(a)]. This Fe state, with no orbital degree of freedom, is consistent with previous studies on other Fe-substituted manganites.¹³ For details on the x-ray absorption measurements, see Ref. 14. The Mn $2p$ absorption spectra of LBMF and of a $\text{La}_{0.7}\text{Sr}_{0.3}\text{MnO}_3$ (LSM) single crystal are shown in Fig. 3(b). The shape of the spectrum of LBMF is similar to that of LSM, with a chemical shift of $\sim +0.25$ eV. Since the chemical shift of the Mn $2p$ edge in manganites is $+1.0$ eV/valence unit,¹¹ this result points to an average Mn valence of $\sim +3.55$ for LBMF. The Mn $1s$ absorption spectrum of LBMF is shown in Figs. 3(c) and 3(d). The spectra of LaMnO_3 , CaMnO_3 , both consistent with the literature,¹⁵ and a linear combination $0.55 \times \mu(\text{CaMn}^{4+}\text{O}_3) + 0.45 \times \mu(\text{LaMn}^{3+}\text{O}_3)$ are also given. There is good agreement between such a linear combination and the observed spectrum of LBMF, in particular the inflection point energies at the main edge, giving further support for the average Mn valence $\sim +3.55$. The single-valent Fe and mixed-valent Mn ions in the proportion $0.27\text{Mn}^{3+}:0.34\text{Mn}^{4+}:0.33\text{Fe}^{3+}$ re-

vealed here indicate the presence of ~ 0.3 orbitally active electrons ($\text{Mn}^{3+}e_g^1$) per transition-metal ion in LBMF. Such a relatively dilute orbital concentration is equivalent to that found in electron-doped manganites.

Neutron scattering, magnetic susceptibility, and specific-heat measurements demonstrate a magnetically frustrated ground state with anisotropic (A -type) AFM correlations for LBMF. Such spin correlations cannot be understood in a quasi-cubic perovskite structure unless orbital correlations also take place. Also, the orbital correlation length cannot be smaller than the A -AFM spin counterpart, being therefore inferred to be larger than ~ 30 Å at low T [see Fig. 2(d)]. Further, the conspicuous thermal behavior of the lattice parameters and atomic distances [Figs. 2(e) and 2(f)], suggests that such correlations might be long ranged, defining an OO state.

It is relevant to ask whether the A -AFM and by extension the orbital correlations observed here might be associated with local fluctuations of the chemical composition. This scenario might lead to Mn^{3+} -rich clusters where orbital correlations (with related A -AFM spin correlations) would be more prone to develop. Below we argue against this scenario. In fact, the low T specific heat appears to be dominated by spin excitations associated with the A -AFM structure [see Fig. 1(c)], indicating that a large volume fraction of the sample is in such a magnetic state at low T . Also, the A -AFM correlation length ξ would be expected to be nearly T independent in this scenario, i.e., given by the size of the Mn^{3+} -rich chemical cluster. Instead, ξ increases significantly on cooling, from ~ 10 Å at 150 K to ~ 30 Å at 10 K [see Fig. 2(d)]. We conclude that compositional fluctuations, although probably present to a certain degree in our sample, are not responsible for the unusual properties of LBMF reported in this work. The results shown in Fig. 2(d) actually indicate that the A -AFM spin correlations, favored by the presumably more robust orbital correlations over the whole bulk, are blocked by the large exchange disorder caused by Fe^{3+} substitution, thus preventing the development of a long-range spin-ordered state. Upon cooling, the free energy of the A -AFM state becomes increasingly favorable, leading to a gradual increase of ξ .

The survival of significant orbital correlations in an environment of large chemical/exchange disorder may help to elucidate the relevant mechanisms of OO in manganites. In fact, it seems rather unlikely that such correlations amongst dilute orbitals would be observed in such a disordered system if the orbital interactions were short ranged (nearest neighbor) such as implied by the exchange mechanism. Thus, our results support an anisotropic strain field mechanism.⁴ Such a field, for being long ranged,¹⁶ is more likely able to overcome the local disorder introduced by the Fe substitution and lead to the robust orbital correlations observed in this work.

We thank C. Piamonteze and F.M.F. de Groot for helpful discussions. This work was partly supported by Fapesp and CNPq, Brazil. Work at the University of Maryland was supported by the NSF-MRSEC, DMR-05-20471. Work at Minsk was partly supported by BRFFI Grant No. 04P-163.

*Electronic address: egranado@ifi.unicamp.br

- ¹Y. Tokura and N. Nagaosa, *Science* **5465**, 462 (2000).
- ²E. O. Wollan and W. C. Koehler, *Phys. Rev.* **100**, 545 (1955); J. B. Goodenough, *Phys. Rev.* **100**, 564 (1955).
- ³K. I. Kugel and D. I. Khomskii, *JETP Lett.* **15**, 446 (1972); *Sov. Phys. JETP* **37**, 725 (1973); *Sov. Phys. Usp.* **25**, 231 (1982).
- ⁴D. I. Khomskii and K. I. Kugel, *Phys. Rev. B* **67**, 134401 (2003).
- ⁵S. N. Barilo *et al.*, *J. Cryst. Growth* **211**, 480 (2000).
- ⁶F. He and P. J. van Espen, *Anal. Chem.* **63**, 2237 (1991).
- ⁷J. Dho, W. S. Kim, and N. H. Hur, *Phys. Rev. Lett.* **89**, 027202 (2002).
- ⁸High-flux neutron measurements were performed on the BT-7 spectrometer at NIST Center for Neutron Research (NCNR), with fixed incident energy $E_i=13.4$ meV. Pyrolytic graphite monochromator, filter, and analyzer (when applicable) were employed, with relaxed collimations. The energy resolution was ~ 1 meV.
- ⁹B. F. Woodfield, M. L. Wilson, and J. M. Byers, *Phys. Rev. Lett.* **78**, 3201 (1997).
- ¹⁰High-resolution neutron powder diffraction measurements on the grounded crystallites of LBMF were performed on the BT-1 powder diffractometer at NCNR, using a monochromatic beam with $\lambda=1.5402(1)$ Å, produced by a Cu(311) monochromator. Collimations were 15', 20', and 7' arc before and after the monochromator, and before detectors, respectively. The crystal structure was Rietveld refined using the program GSAS [C. Larson and R. B. Von Dreele (unpublished)] and an orthorhombic perovskite model with *Imma* symmetry. The *a* and *c* lattice parameters were found to be nearly the same within our resolution and were subsequently constrained as equal in the structural model, without incrementing the fitting residuals. The cationic concentrations were kept fixed at the values found by x-ray fluorescence measurements; no significant improvement in the fit was obtained when the La/Ba and Mn/Fe ratios were allowed to vary freely. The occupancy in the oxygen sites [$\nu(\text{O})$] was initially refined at 300 K, yielding $\nu(\text{O})=1.04(2)$, and was subsequently fixed at unity for all *T*. The fitting residuals were $R_{pb}=6.4\%$, $R_{wpb}=6.8\%$, and $\chi^2=1.05$ at 300 K, and $R_{pb}=7.2\%$, $R_{wpb}=9.1\%$, and $\chi^2=1.42$ at 10 K (25 variables). The refined lattice and atomic parameters at 300 K are $a=c=5.533\ 04(7)$ Å, $b=7.8475(2)$ Å; La/Ba (0, 1/4, -0.013(2)) with $B_{iso}=0.9(1)$ Å²; Mn/Fe (1/2, 0, 0) with $B_{iso}=3.0(4)$ Å²; O1(1/2, 1/4, 0.032(1)) with $B_{11}=B_{33}=1.9(2)$ Å² and $B_{22}=1.7(2)$ Å²; O2(1/4, -0.0094(6), 1/4) with $B_{11}=B_{33}=0.51(6)$ Å², $B_{22}=2.2(2)$ Å², and $B_{13}=0.9(1)$ Å². Quoted errors are statistical only, and represent one standard deviation. High-resolution x-ray powder diffraction measurements were performed in a limited angular interval covering a few Bragg peaks on the XRD-1 beamline at Laboratório Nacional de Luz Síncrotron (LNLS), using a double-bounce Si(111) monochromator and a Ge(111) analyser, with $\lambda=1.282$ Å. The lattice parameters below and above room temperature were obtained using neutron and x-ray data, respectively.
- ¹¹M. Abbate *et al.*, *Phys. Rev. B* **46**, 4511 (1992).
- ¹²For a review, see F. de Groot, *Chem. Rev. (Washington, D.C.)* **101**, 1779 (2001).
- ¹³G. H. Jonker, *Physica (Amsterdam)* **20**, 1118 (1954); A. Simopoulos *et al.*, *Phys. Rev. B* **59**, 1263 (1999).
- ¹⁴Soft x-ray absorption spectroscopy (XAS) measurements at the Mn and Fe 2*p* edges were performed on the beamline SGM at LNLS, using a spherical grating monochromator with energy resolution ~ 0.6 eV (FWHM). The spectra were collected in the total-electron-yield mode, the incident beam being focused on a fresh broken surface of the LBMF crystal. A single crystal of La_{0.7}Sr_{0.3}MnO₃ was used as a reference sample for the Mn 2*p* edge [E. Granado *et al.*, *Phys. Rev. B* **58**, 11435 (1998)]. A simulation for the Fe 2*p* edge was performed using the crystal-field multiplet approach (Ref. 12), using 45% and 63% of the atomic values for the *dd* and *pd* Slater integrals, respectively, and a crystal-field splitting between *t*_{2*g*} and *e*_g states of 10*Dq* = 1.5 eV for point group *O_h*. Hard-XAS measurements were carried out on the XAS beamline at LNLS, using a double-bounce Si(111) monochromator. The energy resolution was better than ~ 2.0 eV (FWHM). The spectra were collected in transmission mode. A ceramic sample of CaMnO₃ grown by conventional solid-state reaction, and a single crystal of LaMnO_{3,00} grown by optical floating zone method, were used as reference samples.
- ¹⁵G. Subías *et al.*, *Phys. Rev. B* **56**, 8183 (1997); F. Bridges *et al.*, *ibid.* **61**, R9237 (2000); **63**, 214405 (2001); A. Yu. Ignatov, N. Ali, and S. Khalid, *ibid.* **64**, 014413 (2001).
- ¹⁶J. D. Eshelby, in *The Continuum Theory of Lattice Defects in Solid State Physics*, edited by F. Seitz and D. Turnbull (Academic Press, New York, 1956); D. I. Khomskii and K. I. Kugel, *Europhys. Lett.* **55**, 208 (2001).